

Rotational Variability and Detection of Superflares in a Young Brown Dwarf by TESS

Rajib KUMBHAKAR, Soumen MONDAL*, Samrat GHOSH, Diya RAM and Sudip PRAMANIK

S. N. Bose National Centre for Basic Sciences, Salt Lake, Kolkata 700106, India

* Corresponding authors: rajskbuph0@gmail.com; soumen.mondal@bose.res.in

Abstract

We present a comprehensive analysis of a Transiting Exoplanet Survey Satellite (TESS) high-quality light curve for a young brown dwarf, MHO 4 having spectral type M7.0, in the Taurus star-forming region. We investigate the rotation periods and characterize the BD's dynamic atmosphere and surface features. We present light curve analysis of MHO 4, and estimate the rotation period to be around 2.224 d. Remarkably, MHO 4 exhibits two significant flaring events. Furthermore, we also estimated bolometric flare energies to be within the energy range of 10^{34} to 10^{35} erg, which sits in the superflare category.

Keywords: brown dwarfs, TESS, photometric variability, periodic variables, starspots

1. Introduction

Brown dwarfs (BDs) were initially theorized by Shiv Kumar in 1962 (Joergens, 2014) and so far thousands of BDs have been discovered (Martín et al., 1999; Carnero Rosell et al., 2019). BDs occupy an intermediate-mass range between planets and stars, typically ranging from approximately 13 to 80 times the mass of Jupiter. Due to their low masses, they can not sustain nuclear fusion by burning hydrogen inside their core; instead, they burn deuterium. Being cool and fully convective, BDs show different kinds of atmospheric features and cause modulation of flux as it rotates, which can be interpreted by studying the light curve. Therefore, photometric variability is an important tool for studying their surface characteristics and atmospheric properties.

In recent years, variability of these objects has been observed over a broad range of wavelengths (Carpenter et al., 2001; Ghosh et al., 2021; Wang et al., 2023). In the optical range, photometric variability of BDs mainly arises due to the rotational modulation of active starspots regions in the photosphere, along with magnetically induced chromospheric activity at higher altitudes in the atmosphere, dust clouds, or binary companions. Thus variability can probe the diverse set of several physical mechanisms for these classes of young objects and study diverse environments. With age, the shape of light curves of young objects, their rotation periods, and surface features in the photosphere has been investigated by the availability of high-cadence and high-precision photometric observations from spacecraft such as CoRoT (Baglin et al., 2006),

MOST (Matthews et al., 2000), and Kepler extended mission K2 (Howell et al. (2014)). Here we used the Transiting Exoplanet Survey Satellite (TESS; Ricker et al. (2015)), which also has high-cadence, high-precision light curves of young objects, covering many young clusters, including the extended Taurus star-forming region with wavelength range from 600 to 1000 *nm*.

In this study, we presented the analysis of TESS photometric data of a young BD, MHO 4 (TIC 456944264) with spectral type M7.0 (White and Basri, 2003). It is a bonafide member of the young Taurus star-forming region. We further analyze the power spectrum to infer the rotation periods and the physical mechanism behind stellar flares. Section 2 describes the TESS observation and data analysis procedure, including period analysis. In Section 3, we presented the light curve of our source and described flare analysis and the results derived from them. Finally, in Section 4, we summarized the key findings of our study.

2. TESS Observations and Data Analysis

We used the time-series data of TESS, which is briefly discussed here (for more details, please see Ricker et al. 2015). TESS is a space-based telescope launched by NASA in April 2018. It consists of four cameras with a size of 10 cm and a combined field of view $24^\circ \times 96^\circ$. During the first extended mission, TESS observed our selected object, MHO 4, in both TESS sector 43 (Camera 3 and CCD 3) and sector 44 (Camera 2, CCD 4). We used 2-min cadence photometry, publicly accessible through the Mikulski Archive for Space Telescopes (MAST). We use `lightkurve` (Lightkurve Collaboration et al., 2018) package to download the lightcurve of MHO 4 from MAST. These data were already processed by the Science Processing Operations Center (SPOC), and we used Pre-search Data Conditioning Simple Aperture Photometry (PDCSAP) flux for our analysis. PDCSAP light curves are generated light curves from SAP flux, which are removed of systematics effects using the Presearch Data Conditioning (PDC) pipeline module (see more details: Jenkins et al. 2016). Additionally, we utilize the 'hardest' bitmask filter in `lightkurve` and then filtered the data by removing outliers and NaNs values and further normalized the light curves by dividing each flux by its mean.

Visual inspection of the PDCSAP light curve of MHO 4 in Figure 1 displays a variable nature over the sectors. Figure 1 also shows the periodogram and phase folded light curve of MHO 4. Here, we utilized two independent techniques to infer the rotation period of MHO 4 using TESS data, i.e., Lomb-Scargle periodogram (VanderPlas, 2018) and Gaussian Process (GP) (Angus et al., 2018). We used `lightkurve.periodogram` to estimate the object's period, and the phase curve is constructed using the most significant peaks in the periodogram. We also attempted to infer the rotation period using the GP method and provided a posterior probability distribution function that can be utilized to estimate rotation periods' uncertainty. Furthermore, for the GP method, we used `exoplanet` (Foreman-Mackey et al., 2021) and `celerite2` (Foreman-Mackey, 2018) package to model rotation periods in each Sectors individually. We elected to use `PyMc3` package for posterior distribution as it offers several general models. The estimated rotation periods of MHO 4 from TESS 2-min cadence data are described in Section 3. Furthermore, `Allesfitter` code is utilized to model the detected complex flare events of MHO 4 via Bayesian evidence.

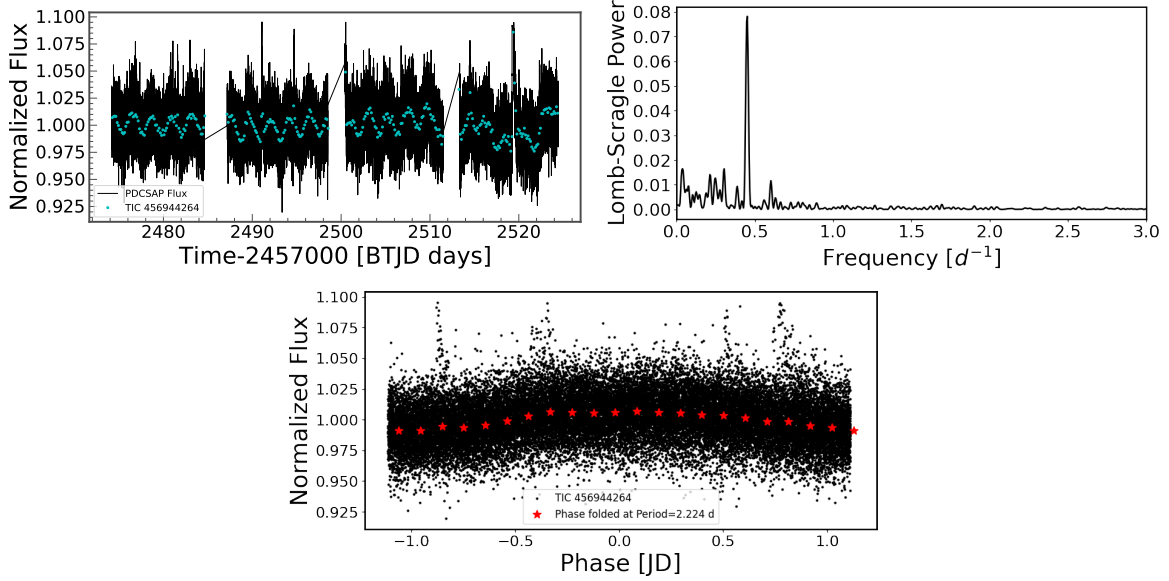


Figure 1: The TESS PDCSAP light curve (upper-left panel), LS periodogram (upper-right panel) and phase folded light curve (lower panel) of MHO 4 are shown here. Blue dots in the light curve represent the binning points of 200-min and red dots are the 150-min binning points in the phase curve.

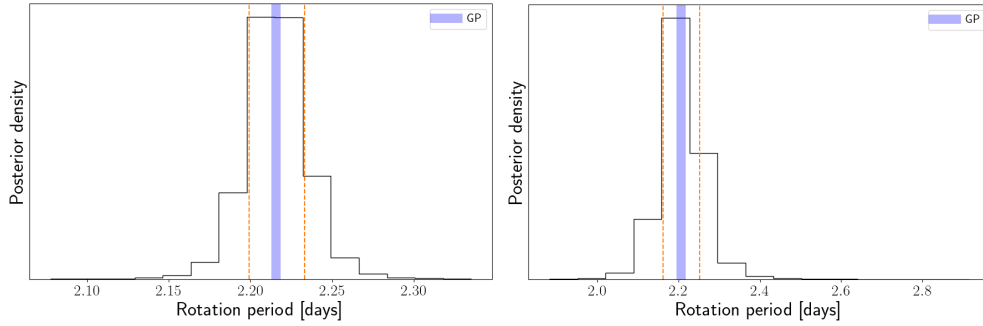


Figure 2: Posterior models of rotation periods of MHO 4, measured from TESS 2-min cadence data, is shown here. The blue line represents the rotation periods and the orange lines are the uncertainties to the periods.

3. Results and Discussions

MHO 4 is a young BD having spectral type M7.0, $T_{eff} = 2814$ K, $R = 0.655R_{\odot}$ (Stassun et al., 2018), belonging to the Taurus association. Previously, Briceño et al. (1998) identified strong Li I $\lambda 6707$ absorption line along with He I $\lambda 5876$, [O I] $\lambda 6300$, [O I] $\lambda 6363$ for this object. Rebull et al. (2020), using the K2 observation, reported the period around 2.2098 d while Güdel et al. (2007) recorded the upper limit of the rotation period as 6.29 d based on X-ray observation with the XMM-Newton data. Figure 1 illustrates the TESS light curve, LS periodogram, and phase curve of MHO 4 stitched to both sectors. We measured the rotation period using the LS method to be 2.224 d, and when analyzing each TESS sector separately, we also got consistent periods. The estimated rotation period using GP method is $2.215^{+0.017}_{-0.016}$ d in sector 43 and $2.205^{+0.047}_{-0.043}$ d in sector 44. The rotation periods derived from these two independent methods exhibit reasonably close values. The posterior distribution of rotation periods of MHO 4 for both sectors are shown in Figure 2.

Table 1: The details of flare properties of MHO 4

Object	Sector	Radius	Temperature (K)	Rel. Amplitude	ED (sec)	Energy (erg)	Duration (min)
MHO 4	43	0.655	2814.0	0.857	1479.79 ± 11.10	$4.01\text{E}+34$	84
"	44	0.655	2814.0	1.209	5852.15 ± 22.17	$1.59\text{E}+35$	298

Note: Radius and temperature are taken from Stassun et al. (2018) and amplitude (rel. flux) and EDs were computed using Altaipony software.

3.1. Flare Detection and Analysis

As a result of flare detection, we have identified one flares from each sector of MHO 4. For example, we presented the PDCSAP and detrended light curve for sector 44 in Figure 3. Initially, we inspected visually and reconfirmed the detection of flares by an open source *Python*

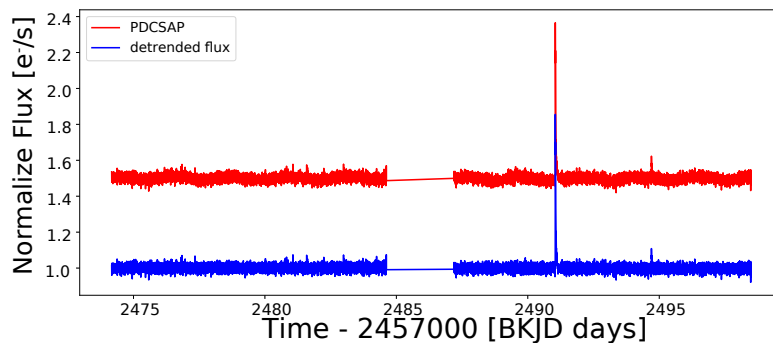


Figure 3: The PDCSAP and detrended light curves of MHO 4 for sector 44 are shown here. The x-axis is the time in Barycentric Kepler Julian Days (BKJD), and the y-axis is the normalized TESS flux (e^-/s). Red highlights PDCSAP data. Blue gives the detrended flux (e^-/s) with no intrinsic variation present..

software ALTAIPONY (Ilin, 2021). This software provides several flare parameters, like i.e., start and stop time, flare amplitude, and equivalent duration (ED). To estimate the bolometric flare energy, we used the equation defined by Shibayama et al. (2013) and Ikuta et al. (2023). Assuming the flare as a blackbody of temperature 10,000 K, we calculated flare energy as 4.01×10^{34} erg in sector 43 and 1.59×10^{35} erg in sector 44. Table 1 describes the details of flare parameters.

Generally, flare light curves in BDs exhibit a rapid rise and gradual decline in brightness. However, all flare light curves show multi-peaked behaviour in the decline phase suggesting such flare events are complex. We further analyzed and modeled these flare light curves using open-source package Allesfitter (Günther and Daylan, 2021) We modeled the flare light curve using the Nested Sampling (Skilling, 2006) algorithm, which provides the flares' peak times, amplitudes and FWHMs, white noise scaling, and a constant baseline. As a preliminary result, we found two flare candidate peaks in Sector 43, while in Sector 44, four flare candidate peaks fitted well to the flares. Figure 4 illustrates the fitted flare light curve and their residuals. Figure 5 shows the posterior probability distribution of flare parameters.

Inspecting the power spectrum and phase light curve of MHO 4, we identified a significant

peak in the LS periodogram. Folding the light curve at this period revealed a clear, smooth variation across the different sectors. Such smooth variations are typically associated with rotational modulation mainly of the spots or groups of spots with the objects (Rebull et al., 2016). So, here we deduced the mean spot temperature T_{spot} of MHO 4 using a quadratic formula proposed by Herbst et al. (2021), $T_{spot} = -3.58 \times 10^{-5} T_{eff}^2 + 0.801 \times T_{eff} + 666.5$

Additionally, We illustrated the spot relative intensity f_{spot} for the TESS band, which depends on the stellar effective temperature T_{eff} and the spot temperature, T_{spot} : $f_{spot} = \frac{\int R_{\lambda} B_{\lambda}(T_{spot}) d\lambda}{\int R_{\lambda} B_{\lambda}(T_{eff}) d\lambda}$

By applying these equations, we estimated the mean spot temperature of MHO 4 to be approximately 2638 K, with a spot relative intensity of approximately 0.65.

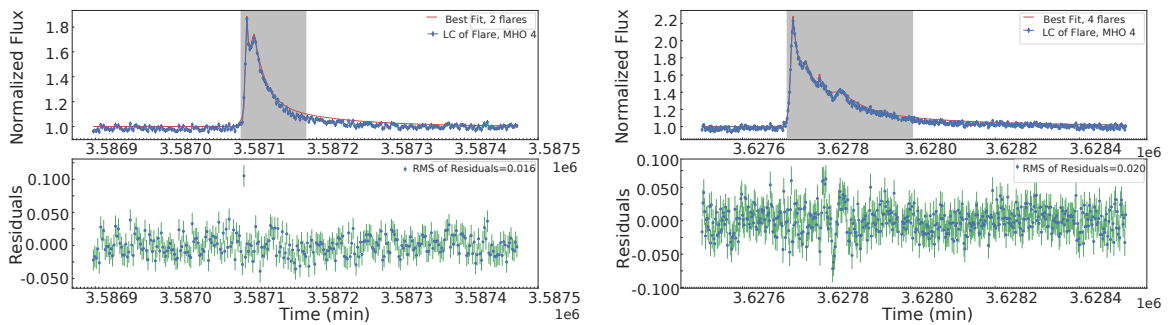


Figure 4: Top: The model fitted the flare light curve of MHO 4 in sector 43 (left) and sector 44 (right) using *Allesfitter*. Blue points are TESS 2-min observational cadence data, and the red line denotes the best-fitted curve. The x-axis shows the time in minutes y-axis shows the PDCSAP flux. Grey span indicates the region of the duration of flares. The below panel shows the residuals of the fitted light curves, and RMS values of the residual are shown in the legend.

4. Summary

In this work, we investigated the photometric variability of a Taurus young BD, MHO 4, using the TESS 2-min cadence data to search for the rotation periods and atmospheric properties. From the analysis of the TESS data, we determined that MHO 4 has a rotation period of approximately 2.224 d, and its phase light curve exhibited smooth variations, which signified rotational modulation of asymmetrically distributed starspots/ groups of spots on its surface. We used two independent techniques, the Lomb-Scargle periodogram and the Gaussian process method, to infer the rotation periods, both yielding consistent results. In addition, we detected two superflare events from MHO 4. The estimated bolometric energies of these flares were 4.01×10^{34} erg (sector 43) and 1.59×10^{35} erg (sector 44). Finally, to model the flare light curves, we observed that the flare in sector 43 was fitted with two flare candidate peaks, while four flare candidate peaks were needed to fit well in sector 44.

Acknowledgments

We would like to thank Dr. Priya Hasan, the referee, for her valuable comments, suggestions on our paper which helped to improve the manuscript. This research work is supported by the S.N.

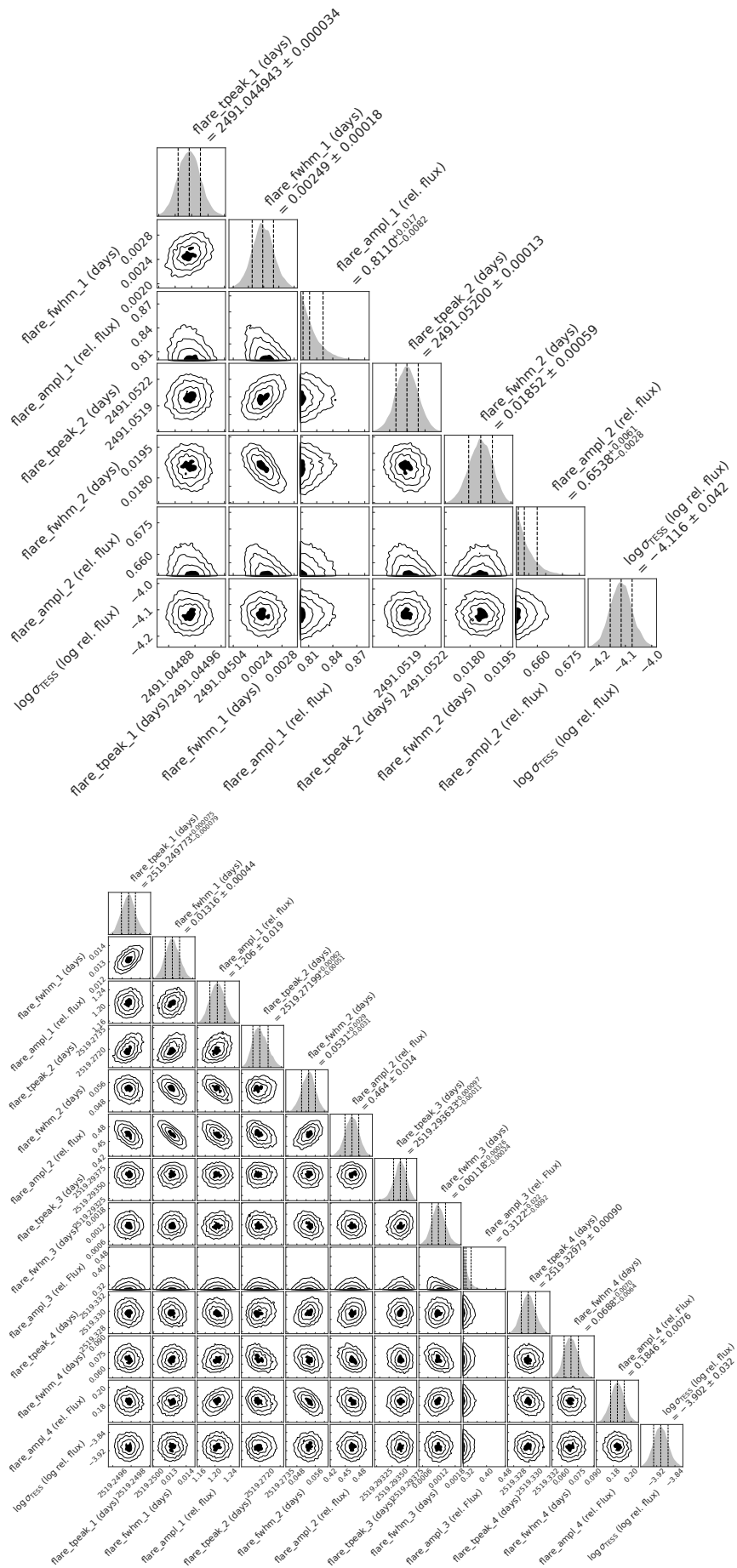


Figure 5: The posterior probability distribution of the flared light curve model parameters for sector 43 (left) and sector 44 (right).

Bose National Centre For Basic Sciences under the Department of Science and Technology, Govt. of India. This paper includes data collected with the TESS mission, obtained from the MAST data archive at the Space Telescope Science Institute (STScI). Funding for the TESS mission is provided by the NASA Explorer Program. STScI is operated by the Association of Universities for Research in Astronomy, Inc., under NASA contract NAS 5-26555. RK is grateful to the Department of Science and Technology (DST), Govt. of India, for their INSPIRE Fellowship scheme.

Further Information

ORCID identifiers of the authors

0000-0001-7277-2577 (Rajib KUMBHAKAR)

0000-0003-1457-0541 (Soumen MONDAL)

0000-0003-3354-850X (Samrat GHOSH)

Author contributions

The light curves and power spectrum analysis were carried out by RK, SM and SG. The examination of the flare analysis part was performed by SG and RK. The text was written by RK. All of the authors provided input on the written draft of the manuscript as well as the discussion and interpretation of the findings.

Conflicts of interest

The authors declare no conflict of interest.

References

- Angus, R., Morton, T., Aigrain, S., Foreman-Mackey, D. and Rajpaul, V. (2018) Inferring probabilistic stellar rotation periods using Gaussian processes. *MNRAS*, 474(2), 2094–2108. <https://doi.org/10.1093/mnras/stx2109>.
- Baglin, A., Auvergne, M., Boisnard, L., Lam-Trong, T., Barge, P., Catala, C., Deleuil, M., Michel, E. and Weiss, W. (2006) CoRoT: a high precision photometer for stellar evolution and exoplanet finding. In 36th COSPAR Scientific Assembly, vol. 36, p. 3749.
- Briceño, C., Hartmann, L., Stauffer, J. and Martín, E. (1998) A Search for Very Low Mass Pre-Main-Sequence Stars in Taurus. *AJ*, 115(5), 2074–2091. <https://doi.org/10.1086/300338>.
- Carnero Rosell, A., Santiago, B., dal Ponte, M., Burningham, B., da Costa, L. N., James, D. J., Marshall, J. L., McMahan, R. G., Bechtol, K., De Paris, L., Li, T., Pieres, A., García-Bellido, J., Abbott, T. M. C., Annis, J., Avila, S., Bernstein, G. M., Brooks, D., Burke, D. L.,

- Carrasco Kind, M., Carretero, J., De Vicente, J., Drlica-Wagner, A., Fosalba, P., Frieman, J., Gaztanaga, E., Gruendl, R. A., Gschwend, J., Gutierrez, G., Hollowood, D. L., Maia, M. A. G., Menanteau, F., Miquel, R., Plazas, A. A., Roodman, A., Sanchez, E., Scarpine, V., Schindler, R., Serrano, S., Sevilla-Noarbe, I., Smith, M., Sobreira, F., Soares-Santos, M., Suchyta, E., Swanson, M. E. C., Tarle, G., Vikram, V., Walker, A. R. and DES Collaboration (2019) Brown dwarf census with the Dark Energy Survey year 3 data and the thin disc scale height of early L types. *MNRAS*, 489(4), 5301–5325. <https://doi.org/10.1093/mnras/stz2398>.
- Carpenter, J. M., Hillenbrand, L. A. and Skrutskie, M. F. (2001) Near-Infrared Photometric Variability of Stars toward the Orion A Molecular Cloud. *AJ*, 121(6), 3160–3190. <https://doi.org/10.1086/321086>.
- Foreman-Mackey, D. (2018) Scalable Backpropagation for Gaussian Processes using Celerite. *Research Notes of the American Astronomical Society*, 2(1), 31. <https://doi.org/10.3847/2515-5172/aaaf6c>.
- Foreman-Mackey, D., Luger, R., Agol, E., Barclay, T., Bouma, L. G., Brandt, T. D., Czekala, I., David, T. J., Dong, J., Gilbert, E. A., Gordon, T. A., Hedges, C., Hey, D. R., Morris, B. M., Price-Whelan, A. M. and Savel, A. B. (2021) exoplanet: Gradient-based probabilistic inference for exoplanet data & other astronomical time series. *arXiv*, arXiv:2105.01994.
- Ghosh, S., Mondal, S., Dutta, S., Das, R., Joshi, S., Lata, S., Khata, D. and Panja, A. (2021) Fast photometric variability of very low mass stars in IC 348: detection of superflare in an M dwarf. *MNRAS*, 500(4), 5106–5116. <https://doi.org/10.1093/mnras/staa3574>.
- Güdel, M., Briggs, K. R., Arzner, K., Audard, M., Bouvier, J., Feigelson, E. D., Franciosini, E., Glauser, A., Grosso, N., Micela, G., Monin, J. L., Montmerle, T., Padgett, D. L., Palla, F., Pillitteri, I., Rebull, L., Scelsi, L., Silva, B., Skinner, S. L., Stelzer, B. and Telleschi, A. (2007) The XMM-Newton extended survey of the Taurus molecular cloud (XEST). *A&A*, 468(2), 353–377. <https://doi.org/10.1051/0004-6361:20065724>.
- Günther, M. N. and Daylan, T. (2021) Allesfitter: Flexible Star and Exoplanet Inference from Photometry and Radial Velocity. *ApJS*, 254(1), 13. <https://doi.org/10.3847/1538-4365/abe70e>.
- Herbst, K., Papaioannou, A., Airapetian, V. S. and Atri, D. (2021) From Starspots to Stellar Coronal Mass Ejections—Revisiting Empirical Stellar Relations. *ApJ*, 907(2), 89. <https://doi.org/10.3847/1538-4357/abcc04>.
- Howell, S. B., Sobeck, C., Haas, M., Still, M., Barclay, T., Mullally, F., Troeltzsch, J., Aigrain, S., Bryson, S. T., Caldwell, D., Chaplin, W. J., Cochran, W. D., Huber, D., Marcy, G. W., Miglio, A., Najita, J. R., Smith, M., Twicken, J. D. and Fortney, J. J. (2014) The K2 Mission: Characterization and Early Results. *PASP*, 126(938), 398. <https://doi.org/10.1086/676406>.
- Ikuta, K., Namekata, K., Notsu, Y., Maehara, H., Okamoto, S., Honda, S., Nogami, D. and Shibata, K. (2023) Starspot Mapping with Adaptive Parallel Tempering. II. Application to

- TESS Data for M-dwarf Flare Stars AU Microscopii, YZ Canis Minoris, and EV Lacertae. *ApJ*, 948(1), 64. <https://doi.org/10.3847/1538-4357/acbd36>.
- Ilin, E. (2021) AltaiPony - Flare science in Kepler, K2 and TESS light curves. *The Journal of Open Source Software*, 6(62), 2845. <https://doi.org/10.21105/joss.02845>.
- Jenkins, J. M., Twicken, J. D., McCauliff, S., Campbell, J., Sanderfer, D., Lung, D., Mansouri-Samani, M., Girouard, F., Tenenbaum, P., Klaus, T., Smith, J. C., Caldwell, D. A., Chacon, A. D., Henze, C., Heiges, C., Latham, D. W., Morgan, E., Swade, D., Rinehart, S. and Vanderspek, R. (2016) The TESS science processing operations center. In *Software and Cyberinfrastructure for Astronomy IV*, edited by Chiozzi, G. and Guzman, J. C., vol. 9913 of *Society of Photo-Optical Instrumentation Engineers (SPIE) Conference Series*, p. 99133E. <https://doi.org/10.1117/12.2233418>.
- Joergens, V. (2014) The Theoretical Prediction of the Existence of Brown Dwarfs by Shiv S. Kumar. In *50 Years of Brown Dwarfs*, edited by Joergens, V., vol. 401 of *Astrophysics and Space Science Library*, p. 1. https://doi.org/10.1007/978-3-319-01162-2_1.
- Lightkurve Collaboration, Cardoso, J. V. d. M., Hedges, C., Gully-Santiago, M., Saunders, N., Cody, A. M., Barclay, T., Hall, O., Sagar, S., Turtelboom, E., Zhang, J., Tzanidakis, A., Mighell, K., Coughlin, J., Bell, K., Berta-Thompson, Z., Williams, P., Dotson, J. and Bar-entsen, G. (2018) Lightkurve: Kepler and TESS time series analysis in Python. *Astrophysics Source Code Library*, record ascl:1812.013.
- Martín, E. L., Delfosse, X., Basri, G., Goldman, B., Forveille, T. and Zapatero Osorio, M. R. (1999) Spectroscopic Classification of Late-M and L Field Dwarfs. *AJ*, 118(5), 2466–2482. <https://doi.org/10.1086/301107>.
- Matthews, J. M., Kuschnig, R., Walker, G. A. H., Pazder, J., Johnson, R., Skaret, K., Shkolnik, E., Lanting, T., Morgan, J. P. and Sidhu, S. (2000) Ultraprecise Photometry from Space: The MOST Microsat Mission. In *IAU Colloq. 176: The Impact of Large-Scale Surveys on Pulsating Star Research*, edited by Szabados, L. and Kurtz, D., vol. 203 of *Astronomical Society of the Pacific Conference Series*, pp. 74–75.
- Rebull, L. M., Stauffer, J. R., Bouvier, J., Cody, A. M., Hillenbrand, L. A., Soderblom, D. R., Valenti, J., Barrado, D., Bouy, H., Ciardi, D., Pinsonneault, M., Stassun, K., Micela, G., Aigrain, S., Vrba, F., Somers, G., Christiansen, J., Gillen, E. and Collier Cameron, A. (2016) Rotation in the Pleiades with K2. I. Data and First Results. *AJ*, 152(5), 113. <https://doi.org/10.3847/0004-6256/152/5/113>.
- Rebull, L. M., Stauffer, J. R., Cody, A. M., Hillenbrand, L. A., Bouvier, J., Roggero, N. and David, T. J. (2020) Rotation of Low-mass Stars in Taurus with K2. *AJ*, 159(6), 273. <https://doi.org/10.3847/1538-3881/ab893c>.
- Ricker, G. R., Winn, J. N., Vanderspek, R., Latham, D. W., Bakos, G. Á., Bean, J. L., Berta-Thompson, Z. K., Brown, T. M., Buchhave, L., Butler, N. R., Butler, R. P., Chaplin, W. J.,

- Charbonneau, D., Christensen-Dalsgaard, J., Clampin, M., Deming, D., Doty, J., De Lee, N., Dressing, C., Dunham, E. W., Endl, M., Fressin, F., Ge, J., Henning, T., Holman, M. J., Howard, A. W., Ida, S., Jenkins, J. M., Jernigan, G., Johnson, J. A., Kaltenegger, L., Kawai, N., Kjeldsen, H., Laughlin, G., Levine, A. M., Lin, D., Lissauer, J. J., MacQueen, P., Marcy, G., McCullough, P. R., Morton, T. D., Narita, N., Paegert, M., Palle, E., Pepe, F., Pepper, J., Quirrenbach, A., Rinehart, S. A., Sasselov, D., Sato, B., Seager, S., Sozzetti, A., Stassun, K. G., Sullivan, P., Szentgyorgyi, A., Torres, G., Udry, S. and Villaseñor, J. (2015) Transiting Exoplanet Survey Satellite (TESS). *JATIS*, 1, 014003. <https://doi.org/10.1117/1.JATIS.1.1.014003>.
- Shibayama, T., Maehara, H., Notsu, S., Notsu, Y., Nagao, T., Honda, S., Ishii, T. T., Nogami, D. and Shibata, K. (2013) Superflares on Solar-type Stars Observed with Kepler. I. Statistical Properties of Superflares. *ApJS*, 209(1), 5. <https://doi.org/10.1088/0067-0049/209/1/5>.
- Skilling, J. (2006) Skilling, j.: Nested sampling for general bayesian computation. *bayesian anal.* 1(4), 833-860. *BayAn*, 1, 833–860. <https://doi.org/10.1214/06-BA127>.
- Stassun, K. G., Oelkers, R. J., Pepper, J., Paegert, M., De Lee, N., Torres, G., Latham, D. W., Charpinet, S., Dressing, C. D., Huber, D., Kane, S. R., Lépine, S., Mann, A., Muirhead, P. S., Rojas-Ayala, B., Silvotti, R., Fleming, S. W., Levine, A. and Plavchan, P. (2018) The TESS Input Catalog and Candidate Target List. *AJ*, 156(3), 102. <https://doi.org/10.3847/1538-3881/aad050>.
- VanderPlas, J. T. (2018) Understanding the Lomb-Scargle Periodogram. *ApJS*, 236(1), 16. <https://doi.org/10.3847/1538-4365/aab766>.
- Wang, X.-L., Fang, M., Herczeg, G. J., Gao, Y., Tian, H.-J., Zhou, X.-Y., Zhang, H.-X. and Chen, X.-P. (2023) Variability of Young Stellar Objects in the Perseus Molecular Cloud. *arXiv*, arXiv:2305.02514. <https://doi.org/10.48550/arXiv.2305.02514>.
- White, R. J. and Basri, G. (2003) Very Low Mass Stars and Brown Dwarfs in Taurus-Auriga. *ApJ*, 582(2), 1109–1122. <https://doi.org/10.1086/344673>.